Microchimica Acta (2022) 189: 229
https://doi.org/10.1007/s00604-022-05310-9

ORIGINAL PAPER

Impedimetric aptasensor based on porphyrin-based covalent-organic framework for determination of diethylstilbestrol

Rongyuan Chen[1] · Lun Kan[1] · Mingyang Xu[1] · Geyi Zhang[2] · Minghua Wang[1] · Jing Cui[1] · Nan Zhou[2] · Linghao He[1]

Received: 4 February 2022 / Accepted: 16 April 2022 / Published online: 25 May 2022

Abstract

An impedimetric sensing strategy was developed for sensitively determining diethylstilbestrol (DES) based on a platform of porphyrin-containing covalent-organic framework (p-COF). The p-COF was synthesized using 5,10,15,20-tetra (4-aminophenyl) porphyrin (TAPP) and 1,3,6,8-tetrakis(4-formylphenyl) pyrene (TFPy) as building blocks via condensation reaction, for which p-COF was named as TAPP-TFPy-COF. Considering the large specific surface area (302.9 $m^2 g^{-1}$), high porosity, rich nitrogen functionality, superior electrochemical activity, and strong bioaffinity toward DNA strands, the TAPP-TFPy-COF-based platform exhibited enhanced, non-label, and amplified electrochemical signal, large number of immobilized DES-targeted aptamer strands, and fast-response toward the analyte. Electrochemical results reveal that the TAPP-TFPy-COF-based aptasensor promoted the sensing performance for the detection of DES, resulting in an extremely low limit of detection of 0.42 fg mL^{-1} within a DES concentration ranging from 1 fg mL^{-1} to 0.1 pg mL^{-1}, which was substantially lower than those of most reported DES sensors. Furthermore, the TAPP-TFPy-COF-based aptasensor possessed outperformed stability, high selectivity, ascendant reproducibility, and acceptable applicability in diverse environments. The recovery values for DES detection in milk, tap water, and frozen shrimp were in the range 91.80–118.50% with low relative standard deviation of 0.11–4.26%. This work provides a new sensing electrochemical approach based on COF network for DES detection and shows a deep insight into the construction of COF-based biosensors, which can be extended to be used for other target compounds.

Keywords Impedimetric aptasensor · Porphyrin COF · Covalent-organic framework · Diethylstilbestrol · Electrochemical biosensor

Introduction

Diethylstilbestrol (DES), 4-[(E)-4-(4- hydroxyphenyl)hex-3-en-3-yl] phenol, is a growth promoter in meat-producing animals and fowl, which is vastly applied as clinical medicine [1]. The high-level DES can cause remarkable environmental problem and damage human health. Diverse approaches, such as high-performance liquid chromatography [2], enzyme-linked immunosorbent assay [3], fluorescence [4], gas chromatography–mass spectrometry, electrochemical immunosensors [5], and electrochemiluminescence [6], are being utilized for the detection of DES to control its abuse. However, sophisticated equipment and large number of separate analytical procedures are required, resulting in more complex, time-consuming, and laborious screening procedures [7]. For an efficient probe, DNA aptamer for specific binding with DES has been synthesized and used for DES analysis through electrochemical approaches [8]. In comparison with other electrochemical sensors, aptasensors illustrate some advantages of highly sensitivity, good stability, and low cost.

Diverse nanomaterials, such as conducting polymers [9], conductive nanomaterials [10], and porous-organic frameworks [11], have been employed as sensing platforms for

✉ Jing Cui
Jingcui0116@126.com

✉ Nan Zhou
fcczhoun@zzu.edu.cn

✉ Linghao He
helinghao@zzuli.edu.cn

[1] Henan Provincial Key Laboratory of Surface and Interface Science, Zhengzhou University of Light Industry, No. 136, Science Avenue, Zhengzhou 450001, People's Republic of China

[2] Department of Orthopedics, The First Affiliated Hospital of Zhengzhou University, No. 1, Jianshe East Road, Zhengzhou 450052, People's Republic of China

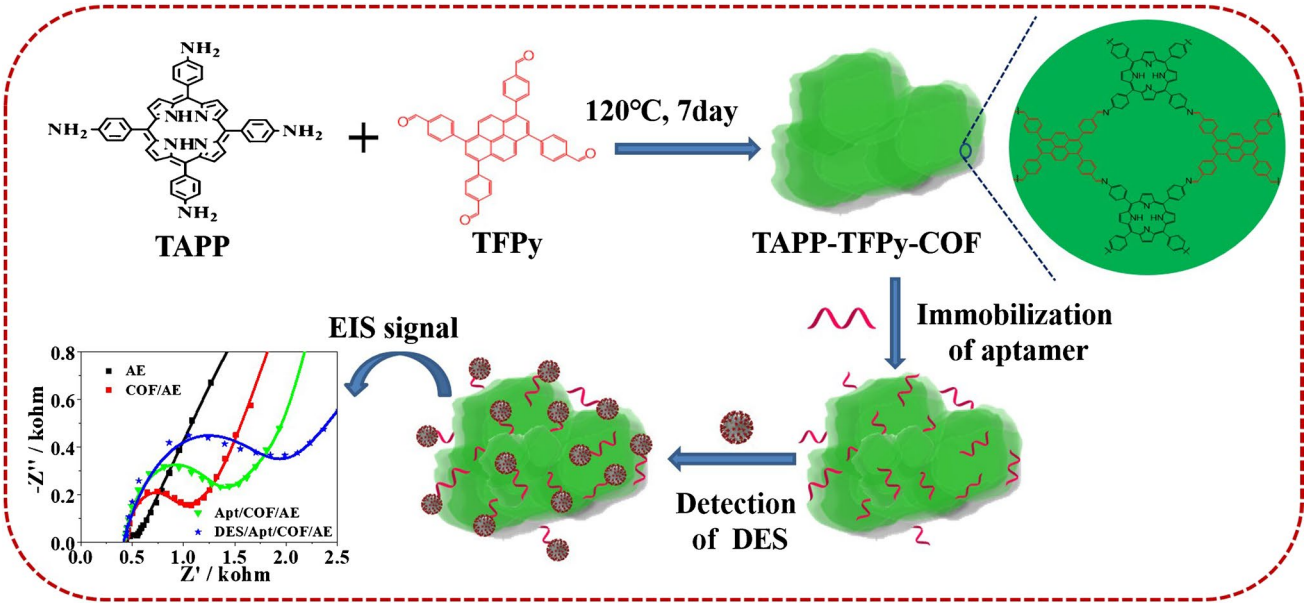

Scheme 1 Schematic diagram of the synthesis of TAPP-TFPy-COF and construction of the TAPP-TFPy-COF-based aptasensor for detecting DES

the construction of biosensors. Covalent-organic frameworks (COFs), as one important category of porous-organic frameworks, are prepared using organic molecules as building blocks into porous networks via covalent bonds [11], which often act as promising candidates for biomedical applications because of abundant functionality [12]. This feature can endow COFs with strong bioaffinity toward diverse kinds of aptamers [11]. Accordingly, some COF-based biosensors have been constructed for detecting different targets. The basic performances of the COF networks depend on their used building blocks. Among different COFs, porphyrinic COFs (p-COFs) comprise highly conjugated π-electron macrocycles, which demonstrate high surface area and electrochemical activity, thus having promising applications as electrode materials for constructing diverse biosensors [13]. Varieties of p-COFs have been prepared and explored as sensing platforms for RNA [14], uracil-DNA glycosylase [15], antibiotics [11], exosome [16], or C-reactive protein [17] detection. Although several samples have been found on the construction of p-COF-based electrochemical sensors, no studies have reported a p-COF-based electrochemical biosensor for the detection of DES.

Considering that the p-COF networks exhibit excellently electrochemical activity, large specific surface area, and high bioaffinity toward the probe molecules, we aimed to develop an electrochemical aptasensor for DES detection based on the porous p-COF network. The p-COF was prepared using TAPP and TFPy as building blocks via condensation polymerization by solvothermal method (Scheme 1). The synthesized TAPP-TFPy-COF was proposed to serve as both the platform for immobilizing the DES-targeted aptamer and electrochemical transducer. Due to highly conjugated structure, superiorly electrochemical activity, and rich functionality of TAPP-TFPy-COF, a large amount of aptamer strands can be adsorbed over the TAPP-TFPy-COF networks via the complex interaction including π-π stacking stacking, electrostatic interaction between aptamer and amino group bearing on COF network, and hydrogen bond [18]. Therefore, the TAPP-TFPy-COF-based aptasensor exhibited excellent sensing performances, such as high sensitivity, good selectivity, and excellent stability. Notably, the constructed TAPP-TFPy-COF-based aptasensor shows wide potential applications for the analysis of DES from different real samples, including seafood, milk, and tap water. In comparison with other electrochemical DES sensors, the sensing strategy based on TAPP-TFPy-COF possesses three innovation points as follows: (i) the feasible construction procedure by directing anchoring DES-targeted aptamer and detecting DES from aqueous solution; (ii) label-free aptamer, no-use of the electroactive redox, and no-blocking by using BSA to further simplify, lower the cost, and shorten the detection time of the development of the aptasensor; (iii) low usage of TAPP-TFPy-COF and good reproducibility of aptasensor afford the TAPP-TFPy-COF-based aptasensor the commercialization application. Consequently, the present work can provide a sensing strategy for the sensitive detection of DES based on the COF networks, which also can be extended to be used in other detection systems when adsorbing different types of probes.

Experimental section

The parts of materials and chemicals, preparation of all solutions, the pretreatment of Au electrode (AE), basic characterization of p-COF, and electrochemical measurements are shown in the S1 section (See the Supplementary Material).

Synthesis of TAPP-TFPy-COF

TAPP-TFPy-COF was synthesized according to the literature through the solvothermal method [19], but with slight modification. The detailed description was provided in the S1.2 section (See the Supplementary Material).

Construction of the TAPP-TFPy-COF-based aptasensor

Ten milligramam of TAPP-TFPy-COF was dispersed in 10 mL of Milli-Q water to form homogeneous dispersion, which were utilized for the assessment of the effect of the COF dosage on the sensing performance. Afterward, 5 µL of TAPP-TFPy-COF dispersion was coated on the pre-treated AE, and naturally dried for 6 h. The constructed TAPP-TFPy-COF-modified AE (denoted as TAPP-TFPy-COF/AE) was stored for further use. Afterward, the TAPP-TFPy-COF/AE was incubated in the aptamer solution (100 nM) at 4 °C for 1 h (represented by Apt/TAPP-TFPy-COF/AE), ensuring the sufficient and saturated immobilization of aptamer over TAPP-TFPy-COF network via the integrated interaction of π-π stacking, Van der Waal force, hydrogen bond, and electrostatic adsorption between negative-charged phosphate group bearing on aptamer and positive-charged amino group of p-COF reserved after condensation reaction. The manufactured aptasensor was stored at 4 °C for further detecting DES. The whole construction procedure of the TAPP-TFPy-COF-based aptasensor and the detection of DES were monitored by electrochemical impedance spectroscopy (EIS) method. The detailed description of electrochemical measurements were provided in the S1.6 section and Fig. S1 (See the Supplementary Material).

Detection of DES Using the TAPP-TFPy-COF-Based Aptasensor

To obtain the optimal experimental conditions, the effects of the concentration of TAPP-TFPy-COF, the concentration of the aptamer, and the binding time toward DES on electrochemical performances TAPP-TFPy-COF-based aptasensor were investigated. The optimal parameters were used for the analysis of DES. The limit of detection (LOD) of the TAPP-TFPy-COF-based aptasensor was determined by separately incubating Apt/TAPP-TFPy-COF/AE in a series of DES solutions with various concentrations (from 1 fg mL^{-1} to 1 ng mL^{-1}). According to the criteria of IUPAC [20], the LOD was deduced from the EIS responses of each measurement.

Furthermore, the selectivity of the TAPP-TFPy-COF-based aptasensor was performed in detecting diverse interferents which may be existed in food pollutants, including antibiotics, such as enrofloxacin (ENR), salbutamol (SAL), zearalenone (ZEA), aflatoxin (AFT), deoxynivalenol (DON), oxytetracycline (OTC), and metal ions (Cr^{3+}, Cu^{2+}, and Ag^{+}). The concentration of interferents were 1 ng mL^{-1}, which is 100-fold of that of DES (10 pg mL^{-1}). In addition, the reproducibility was evaluated by detecting DES (10 pg mL^{-1}) independently using five parallel TAPP-TFPy-COF-based aptasensors. The storage stability was assessed though continuously measuring the DES/Apt/TAPP-TFPy-COF/AE per day after storing at 4 °C for 15 days. Furthermore, the regenerability of TAPP-TFPy-COF-based aptasensor was evaluated by treating the DES/Apt/TAPP-TFPy-COF/AE with 0.05 M NaOH for 2 min and rinsing thoroughly with water. Afterward, the refreshed Apt/TAPP-TFPy-COF/AE was used to detect DES (100 pg mL^{-1}) again. The same procedure was repeated for 15 runs, for which electrochemical responses of the reprocess of the aptasensor and DES detection were recorded.

Applicability of the TAPP-TFPy-COF-based aptasensor

The practical application of the TAPP-TFPy-COF-based aptasensor was performed in diverse situations, including frozen shrimp, milk, and tap water. The frozen shrimp was purchased from the Dazhang supermarket. After spiked with different amounts DES, the frozen shrimp was triturated and further transferred to a 15-mL centrifuge tube. After shaken vigorously by sonication for 1 h, the sample was centrifuged at 1000 rpm for 5 min at room temperature. The supernatant was collected and then dried at 40 °C. Afterward, the solid residue was re-dissolved into 1.0 mL of 50% methanol solution and reconstituted in phosphate buffer (PB) (10 mM) for further use. Milk was purchased from Dazhang supermarket of Zhengzhou. Different amounts of DES were added to milk. Then, milk was treated by adding 0.2 mL of NaOH (0.1 M) and 0.8 mL of acetonitrile, then centrifuging at 5000 rpm for 5 min at room temperature, the supernatant was collected and stored at 4 °C ready for use. Tap water is taken directly from the water pipe. Different amounts of DES were added to tap water. Then, the TAPP-TFPy-COF-based aptasensor was used to analyze the spiked real samples by EIS (see the Electronic Supplementary Material). The electrochemical responses were analyzed according to the calibration curve and compared with the added values.

Results and discussion

Basic characterizations of TAPP-TFPy-COF

The field emission scanning electron microscopy (FE-SEM) images of TAPP-TFPy-COF (Fig. 1a and b) indicates the present of large amounts of nanoparticles, which are loosely stacked together. The corresponding energy dispersive spectroscopy results show that C, N, and O elements are uniformly dispersed in the TAPP-TFPy-COF (Fig. S2). The atomic percentages of each element in all samples are summarized in Table S1. It demonstrates that the atomic percentage of C in TAPP-TFPy-COF is the largest (44.42%), along with 35.88% of N. The transmission electron microscopy (TEM) image (Fig. 1c) suggests that the TAPP-TFPy-COF nanostructure is composed of several flakes with layered structure, in which a few particles were embedded within the nanosheet structure. Generally, the ultrathin COF nanosheets can be aggregated by multiple layers under the influence of π-stacking and hydrogen bonding interaction [21]. No apparent lattice spring can be found in the high-resolution TEM image of TAPP-TFPy-COF (Fig. 1d), revealing the low crystallinity. Furthermore, the X-ray diffraction pattern, FT-IR spectra, the ^{13}C cross-polarization magic-angle spinning NMR spectrum, and N_2 adsorption–desorption isotherms was investigated to analyze the structure and surface area of TAPP-TFPy-COF (Fig. S3). The results were analyzed in the Section S3 of the Electronic Supplementary Material. It suggests that the large specific surface area can improve the fixed amount of aptamer strand, and small size of pore is conducive to the more stable immobilization of the aptamer strand to enhance the detection sensitivity of DES.

The chemical structure and component of TAPP-TFPy-COF were further probed by X-ray photoelectron spectroscopy (XPS). Figure 2a shows that the C 1 *s* XPS spectrum of TAPP-TFPy-COF can be deconvoluted into six parts at the binding energies (BEs) of 283.8, 284.2, 284.5, 285.8, 288.3, and 290.9 eV, which are attributed to C = C, graphite C, C–C, C–N, N–C = O, and π-π* respectively [22]. The coexistence of C = C and weak π-π hints the highly conjugated structure of TAPP-TFPy-COF, which can greatly facilitate the electrochemical activity and boost the binding affinity toward aptamer strands via π-π stacking [11]. Three components were obtained in the N 1 *s* XPS spectrum at the BEs of 397.8, 399.2, and 401.6 eV, corresponding to pyridinic N, pyrrodic N, and graphitic N, respectively. These N-relevant groups bearing on TAPP-TFPy-COF can boost the DNA immobilization [23]. Prior to electrochemical measurements, the change in chemical structure of TAPP-TFPy-COF before and after DNA immobilization was investigated by XPS.

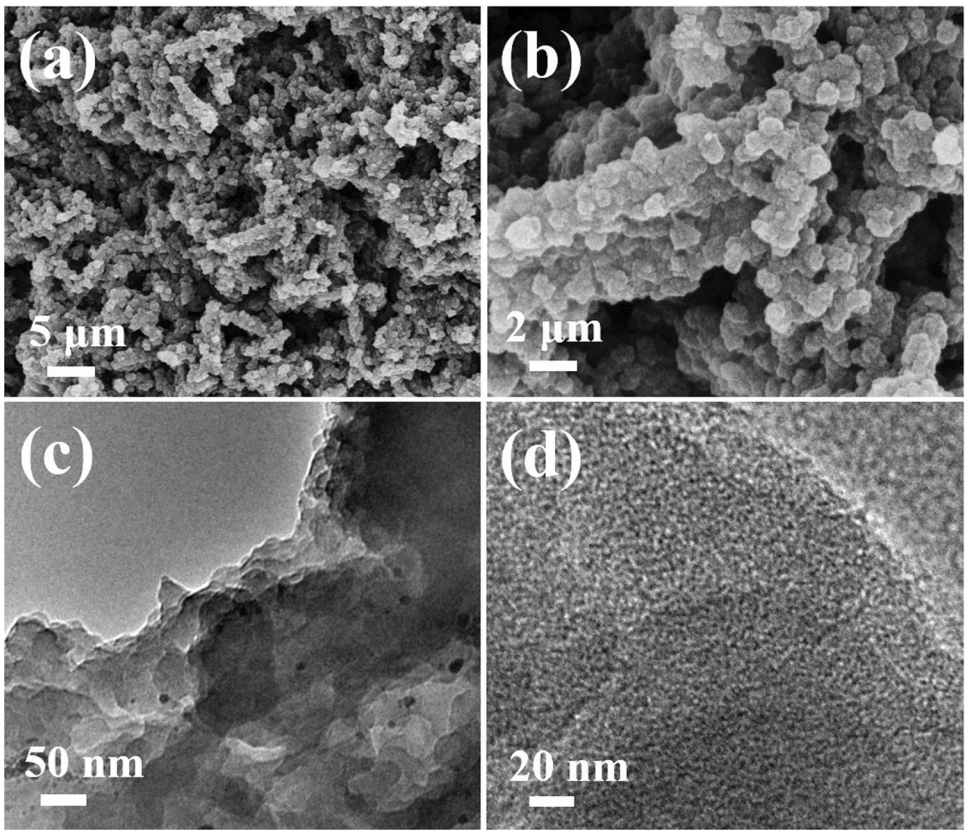

Fig. 1 **a**, **b** Low- and high-magnification SEM and **c**, **d** TEM images of TAPP-TFPy-COF

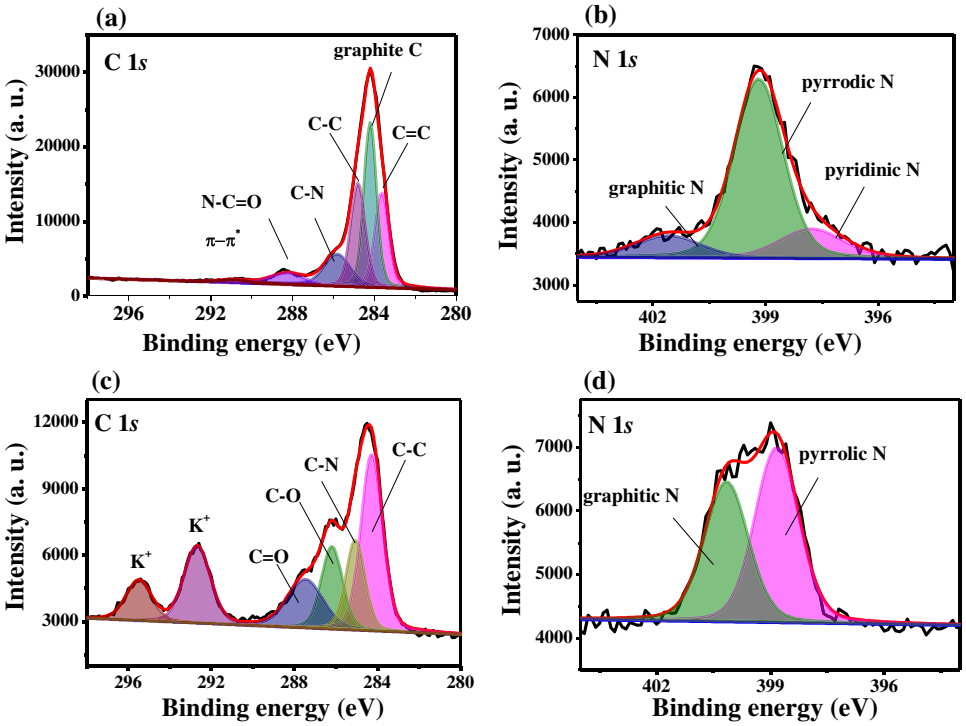

Fig. 2 High-resolution XPS spectra of **a, b** C 1 *s* and N 1 *s* of the TAPP-TFPy-COF and **c**, **d** C 1 *s* and N 1 *s* of the Apt/TAPP-TFPy-COF complex

Figure 2c shows that the C 1 *s* XPS spectrum of the Apt/TAPP-TFPy-COF complex is separated into four groups of C–C, C–N, C–O, and C = O at the BEs of 284.3, 285.1, 286.2, and 287.5 eV, respectively. Besides, two additional peaks at 292.7 and 295.5 eV caused by K^+ are present, which can be attributed to the residual of PB. The C 1 *s* XPS signal generated by C = C group on TAPP-TFPy-COF is absent, while C–O and C = O groups are originated from aptamer strands. Furthermore, two species of pyrrolic N and graphitic N were observed in the N 1 *s* spectrum of the Apt/TAPP-TFPy-COF complex (Fig. 2d). Notably, substantial P 2*p* signal was found, which is an important indicator of the aptamer immobilization and originated from phosphate groups bearing on DNA strands [13, 14]. The P 2*p* XPS spectrum was split into two species at the BEs of 132.9 and 133.9 eV caused by P $2p_{3/2}$ and P $2p_{1/2}$, respectively (Fig. S2f). These findings reveal the successful immobilization of aptamer strands on the TAPP-TFPy-COF networks.

Electrochemical sensing performance of TAPP-TFPy-COF

Figure 3a displays the series EIS Nquist plots of each stage during the construction of the TAPP-TFPy-COF-based aptasensor and DES analysis. The semicircle diameter in Nyquist plots corresponds to the charge transfer resistance (R_{ct}), which reflects the electron transfer kinetics of the redox probe at the electrode surface [17]. The bare AE has a small R_{ct} of 84.8 Ω, revealing the excellent conductivity. After coated with TAPP-TFPy-COF (TAPP-TFPy-COF/AE), a large R_{ct} value of 493.4 Ω was obtained. It indicates that TAPP-TFPy-COF exhibits poorer electrochemical conductivity than that of the bare AE, thus hindering the electron transfer of the electrode/electrolyte interface. However, the R_{ct} value of the TAPP-TFPy-COF/AE is smaller than those of most reported COFs and MOFs (Table S1), hinting the relatively high electrochemical activity. Generally, porphyrin moieties bearing on TAPP-TFPy-COF can greatly enhance electron transfer [13], making it a promising bioplatform for the manufacture of electrochemical aptasensors. After immobilizing aptamer over TAPP-TFPy-COF, the R_{ct} value of the Apt/TAPP-TFPy-COF/AE increased to 851.4 Ω, which is ascribed to the adsorbed aptamers. In aqueous solution, the negatively charged phosphate group on the atpamer was formed, leading to repulsion interaction with $[Fe(CN)_6]^{3-/4-}$, which greatly hampered electron transfer at the solid/solution interface. Subsequently, the R_{ct} value of the electrode increased. When detecting DES, the R_{ct} value of the DES/Apt/TAPP-TFPy-COF/AE continuously increased to 1.44 kΩ, which is attributed to the formed G-quadruplex between DES and aptamer [13]. The insulated aptamer-DES complex further prevented the electron transfer at the electrode/electrolyte interface, which is consistent with other reported sensing COF-based systems [24]. From the impedance data, the coverage (θ) value can be calculated using the equation: $(1-\theta) = R_{ct,i}/R_{ct,i+1}$ [25]. The θ values obtained for aptamer anchored on the TAPP-TFPy-COF/

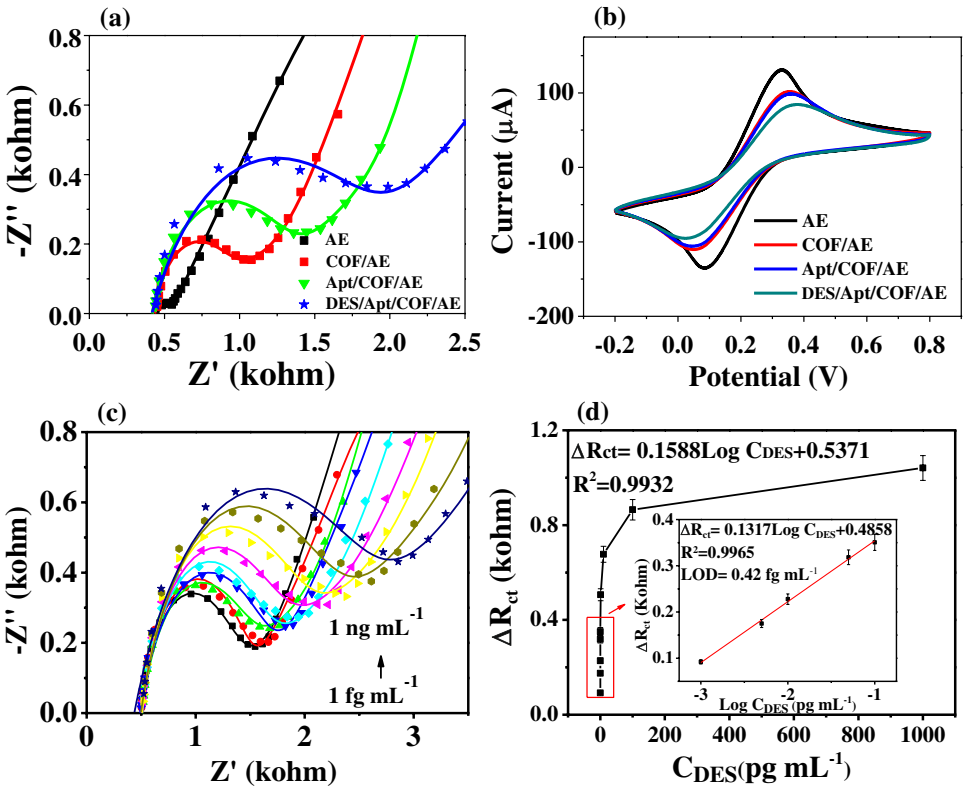

Fig. 3 **a** EIS Nyquist plots and **b** CV curves of the construction of the TAPP-TFPy-COF-based aptasensor for the detection of DES in 0.1 M PB (pH 7.4) containing 5 mM $[Fe(CN)_6]^{3-/4-}$, including (i) AE, (ii) TAPP-TFPy-COF/AE, (iii) Apt/TAPP-TFPy-COF/AE, and (iv) DES/Apt/TAPP-TFPy-COF/AE. **c** EIS responses of the TAPP-TFPy-COF-based aptasensor for the detection of DES with different concentrations (0.001, 0.005, 0.01, 0.05, 0.1, 1, 10, 100, 1000 pg mL^{-1}). **d** Dependence of ΔR_{ct} on the concentration of DES (inset: the linear parts of calibration curves, $n = 3$)

AE and DES adsorbed on the Apt/TAPP-TFPy-COF/AE are 0.42 and 0.41, respectively.

Furthermore, cyclic voltammetry (CV) measurements (Fig. 3b) indicate identical results for the TAPP-TFPy-COF-based aptasensor. The peak current density of the oxidation peak for each stage continuously decreased in the order of bare AE, TAPP-TFPy-COF/AE, Apt/TAPP-TFPy-COF/AE, and DES/Apt/TAPP-TFPy-COF/AE. Therefore, the modification of TAPP-TFPy-COF, immobilization of aptamer, and detection of DES can successively impede the electron transfer, thus decreasing the peak current density [26]. In addition, considering large amounts of aptamer can be immobilized on the porously nanostructured TAPP-TFPy-COF and penetrate into the interior of the COF network; no redundant active sites of TAPP-TFPy-COF was reserved to generate the weak non-specific adsorption of DES. Consequently, blocking agents such as BSA are not required in this novel sensing system. To verify this viewpoint, we constructed the TAPP-TFPy-COF-based aptasensor by using BSA as the blocking step. The adsorption of BSA over the Apt/TAPP-TFPy-COF/AE was measured by EIS (Fig. S4). It reveals that the R_{ct} value of the electrode for the BSA adsorption is 872 Ω, which is comparable to that of the Apt/TAPP-TFPy-COF/AE. Therefore, no substantial adsorption of BSA occurred onto the modified electrode, verifying the above hypothesis.

To obtain the optimal sensing performances of the TAPP-TFPy-COF-based aptasensor for DES detection, the determination conditions for the construction of the biosensor were optimized. As demonstrated in Fig. S5, the optimal conditions for obtaining the superiorly sensing performances of the aptasensor are as follows: dosage of the TAPP-TFPy-COF suspension, 1 mg mL^{-1}; the concentration of the aptamer strands, 100 nM; and binding time for DES with aptamer, 1 h. Under these conditions, EIS measurements were performed for the detection of DES with different concentrations by using the TAPP-TFPy-COF-based aptasensor (Fig. 3c), for which the radius of semi-circles in Nyquist plots increase proportionally to the increase of the DES concentration. This finding can be explained by the G-quadruplex formation between aptamer and DES [8]. The calibration curve of R_{ct} measured for each concentration of DES with repeated measurements of $n = 3$ is illustrated in Fig. 3d. The linear dependence of the change of R_{ct} before and after the detection of DES (ΔR_{ct}) on the logarithm of DES concentration ($LogCon_{DES}$) was determined within the DES concentration from 1 fg mL^{-1} to 1 ng mL^{-1}. In a narrow range from 1 fg mL^{-1} to 0.1 pg mL^{-1}, the corresponding calibration plot of the ΔR_{ct} versus the logarithm of the DES concentration shows a good linear regression equation of the following:

$$\Delta Rct = 0.1317 LogCDES + 0.4858$$

with a square correlation coefficient (R^2) of 0.9965 (inset of Fig. 3d). According to the IUPAC method [20], the LOD is calculated to be 0.42 fg mL^{-1} as follows:

$$\mathrm{LOD} = 3Sb/m$$

in which S_b represents the standard deviation, and m represents the slope in reference to the gradient of calibration graph. In comparison with the other reported sensors for detecting DES (Table 1), the present TAPP-TFPy-COF-based aptasensor exhibits extremely lower LOD for DES detection despite it is suitable for the narrow detection range. Actually, DES can be electrochemically oxidized and thus can be determined by electrochemical techniques [27]. However, these sensors often suffer from low sensitivity for the detection of DES because of the disadvantage of the slow electron transfer of DES. By contrast, the present DES aptasensor based on TAPP-TFPy-COF exhibits low LOD and fast response. That can be ascribed to following factors: (i) the as-synthesized TAPP-TFPy-COF not only can act as the sensitive bioplatform for anchoring a large amount of aptamer via the complex interaction, but also can serve as the electron transducer for boosting the electrochemical response; (ii) the large specific surface area, porous nanostructure, and large pore size of the TAPP-TFPy-COF impel the aptamer to bind both over the surface and into interior of TAPP-TFPy-COF, thus improving the detection sensitivity; and (iii) the relatively large occupation of large aptamer over TAPP-TFPy-COF can avoid the non-specific adsorption between the DES and TAPP-TFPy-COF matrix. Consequently, TAPP-TFPy-COF can serve as a sensitive platform for binding a number of aptamer strands, indicating the superior detection performance of DES.

Apart from the low LOD of the TAPP-TFPy-COF-based aptasensor toward DES, the selectivity of the aptasensor was also investigated by detecting some inferents which possibly co-existed with DES in wastewater, such as other organic pollutants (e.g., ENR, SAL, ZEA, AFT, DON, and OTC) and heavy metal ions (Cr^{3+}, Cu^{2+} or Ag^{+}). Fig. S6a indicates the EIS responses of the separate detection of the TAPP-TFPy-COF-based aptasensor toward different inferents at the concentration of 1000 pg mL^{-1}, which is 100-fold higher than that of DES (10 pg mL^{-1}). The EIS response obtained by testing these inferents can be negligible, while the detection of DES using the aptasensor leads to a substantial response. Moreover, when the TAPP-TFPy-COF-based aptasensor was used to analyze the mixed solution of DES and all interferents, the EIS response is only 4.9% of that of DES. Therefore, the aptasensor illustrates high selectivity in a complex environment.

In addition, the reproducibility and stability of the TAPP-TFPy-COF-based were evaluated toward DES (Figs. S6b–S6d). Five independent electrodes were utilized for the construction of the same aptasensor for DES analysis, for which the EIS responses were obtained, resulting in RSD of 3.25%. Therefore, the TAPP-TFPy-COF-based sensor shows good reproducibility. After continuously testing the same aptasensor for 15 days, the deduced EIS responses were recorded. The result shows a low RSD of 2.75%, hinting the excellent stability of the constructed aptasensor. Furthermore, the regenerated ability of the aptasensor was determined by immersing it in 0.1 M NaOH solution for 2 min. DES molecule was disassociated from the DES-aptamer complex owing to the conformation change in strong base solution. This process resulted in a small EIS response. When the refreshed aptasensor was applied to detect DES again, the EIS response returned a value that is close to the original one. The whole procedure of the regeneration and detection by using the TAPP-TFPy-COF-based aptasensor can be repeated for five runs. Although the number of regeneration is small, it still shows great potential application in real samples.

Table 1 Comparison with other reported techniques for DES detection based on other method

Materials	Detection method	Detection range (ng mL^{-1})	LOD (fg mL^{-1})	Refs
MIP-CdSe/CdS/ZnS QDs	Fluorescence	$50 \sim 2 \times 10^4$	4×10^3	[28]
Lumino-AuNPs@Mo_2C	Electrochemiluminescence	$1 \times 10^{-4} \sim 30$	3.8	[29]
$(Ru(bpy)_{32}+$/UiO-67	Electrochemiluminescence	$1 \times 10^{-5} \sim 50$	3.27	[30]
Silica–Au Nps-MWCNTs	Electrochemical immunosensor	$0.33 \sim 4.5 \times 10^3$	1.2×10^5	[31]
Au/UiO-66(NH_2)/CdS	Photoelectrochemical immunosensor	$1 \times 10^{-4} \sim 20$	60	[32]
AuNPs	Competitive immunoassay	$16 \sim 500$	1.3×10^7	[33]
CdTe NC/rGO	Electrochemiluminescence	$0.002 \sim 2$	1×10^3	[34]
DIB-Cl	HPLC-FLD	$1.5 \sim 300$	5×10^5	[35]
TAPP-TFPy-COF	Electrochemical	$1 \times 10^{-6} \sim 1$	0.37	This work

Real samples

To further investigate the possible application of the TAPP-TFPy-COF-based aptasensor, we applied it for DES detection in three kinds of real samples, including frozen shrimp, milk, and tap water. The original concentration of the target analyte (before the sample being spiked) in the real samples was firstly investigated (Fig. S7). The results show that the ΔR_{ct} of the TAPP-TFPy-COF-based aptasensor before and after the detection of DES in frozen shrim, milk, and tap water is negligible. This finding verifies that no DES exists in real samples. Consequently, the applicability of the developed aptasensor can be assessed by spiking DES solution into real samples. The DES solutions with different concentrations (0.001–1000 pg mL^{-1}) were separately spiked into these real samples, and then detected using the aptasensor and measured using EIS technique. Afterward, the concentrations of the series of DES solutions were deduced according to the calibration curve and compared with the added values. The recovery values for DES detection in frozen shrimp are in the range of 97.12–107.60% with small relative standard deviation (RSD) of 1.96–3.11% (Table 2). Furthermore, the recoveries for the determination of DES in milk and tap water samples were 99.42–117.60% and 95.16–114.5% with low RSDs of less than 4.26% and 2.27%, respectively (Tables S2 and S3). Therefore, the TAPP-TFPy-COF-based aptasensor has great promising application for the real analysis of DES in various environments.

Conclusion

An electrochemical aptasensor was constructed based on porphyrin-COF for DES detection in diverse systems. The synthesized TAPP-TFPy-COF was composed of large amounts of nanoparticles, had high porosity, and displayed highly conjugated structure and rich amino functionality. These features of TAPP-TFPy-COF afforded the superior performances for anchoring a large amounts of aptamer. The TAPP-TFPy-COF-based aptasensor exhibited excellent sensing properties for DES analysis, such as selectivity, stability, and reproducibility. Furthermore, it was verified that the TAPP-TFPy-COF-based aptasensor can be employed to detect DES in diverse environments, such as frozen shrimp, milk, and tap water. The present work provides a deep insight into the construction of the COF-based sensors, which can further widen their applications in different real samples. Nonetheless, the TAPP-TFPy-COF-based aptasensor still presents some unsatisfied features such as poor regenerability and low linear range when detecting DES, which should be addressed in future research.

Supplementary information.

Table 2 Detection of DES in frozen shrimp using the TAPP-TFPy-COF-based aptasensor

Added amount (pg mL^{-1})	Found amount (pg mL^{-1})	Apparent recovery (%)	RSD (%)
0.001	10.76×10^{-4}	107.60	3.11
0.01	10.44×10^{-3}	104.40	2.34
0.1	10.29×10^{-2}	102.96	2.87
1	97.12×10^{-2}	97.12	1.99
10	10.15	101.46	2.26
100	98.41	98.41	1.96
1000	1032.88	103.29	2.44

Supplementary Information The online version contains supplementary material available at https://doi.org/10.1007/s00604-022-05310-9.

Funding This work was supported by the Excellent Youth Science Foundation of Henan Province (202300410494) and the National Natural Science Foundation of China (No. 51903224).

Declarations

Conflict of interest The authors declare no competing interests.

References

1. Lauver D, Nelles KK, Hanson K (2005) The health effects of diethylstilbestrol revisited. Journal of Obstetric, J Obst Gyn Neo 34:494–499
2. Yang Y, Chen J, Shi Y-P (2012) Determination of diethylstilbestrol in milk using carbon nanotube-reinforced hollow fiber solid-phase microextraction combined with high-performance liquid chromatography. Talanta 97:222–228
3. Yang X, Wang Y, Song C, Hu X, Wang F, Zeng X (2020) Hapten synthesis and the development of an ultrasensitive indirect competitive ELISA for the determination of diethylstilbestrol in food samples. Sci Rep 10:3270
4. Zhao C, Jiao Y, Zhang L, Yang Y (2018) One-step synthesis of S, B co-doped carbon dots and their application for selective and sensitive fluorescence detection of diethylstilbestrol. New J Chem 42:2857–2864
5. Zhang S, Du B, Li H, Xin X, Ma H, Wu D, Yan L, Wei Q (2014) Metal ions-based immunosensor for simultaneous determination of estradiol and diethylstilbestrol. Biosens Bioelectron 52:225–231
6. Zhao WR, Kang TF, Xu YH, Zhang X, Liu H, Ming AJ, Lu LP, Cheng SY, Wei F (2020) Electrochemiluminescence solid-state imprinted sensor based on graphene/CdTe@ZnS quantum dots as luminescent probes for low-cost ultrasensing of diethylstilbestrol. Sensor Actuat B-Chem 306:127563
7. Zhao MP, Zhou S, Yan J, Li L (2007) Immunochemical analysis of endogenous and exogenous estrogens. Curr Pharm Anal 3:25–38
8. Li J, Shan X, Jiang D, Chen Z (2020) An ultrasensitive electrochemiluminescence aptasensor for the detection of diethylstilbestrol based on the enhancing mechanism of the metal–organic framework NH_2-MIL-125(Ti) in a 3,4,9,10-perylenetetracarboxylic acid/$K_2S_2O_8$ system. Analyst 145:3306–3312

9. Kaur G, Kaur A, Kaur H (2021) Review on nanomaterials/conducting polymer based nanocomposites for the development of biosensors and electrochemical sensors. Polymer-Plastics Technology and Materials 60:502–519
10. Novodchuk I, Bajcsy M, Yavuz M (2021) Graphene-based field effect transistor biosensors for breast cancer detection: a review on biosensing strategies. Carbon 172:431–453
11. Wang M, Hu M, Liu J, Guo C, Peng D, Jia Q, He L, Zhang Z, Du M (2019) Covalent organic framework-based electrochemical aptasensors for the ultrasensitive detection of antibiotics. Biosens Bioelectron 132:8–16
12. Feng L, Qian C, Zhao Y (2020) Recent advances in covalent organic framework-based nanosystems for bioimaging and therapeutic applications. ACS Mater Lett 2:1074–1092
13. Yan X, Song Y, Liu J, Zhou N, Zhang C, He L, Zhang Z, Liu Z (2019) Two-dimensional porphyrin-based covalent organic framework: a novel platform for sensitive epidermal growth factor receptor and living cancer cell detection. Biosens Bioelectron 126:734–742
14. Gao P, Wang M, Wan X, Liu X, Pan W, Li N, Tang B (2020) A COF-based anti-interference nanoplatform for intracellular nucleic acid imaging. Chem Commun 56:14267–14270
15. Han D, Han Y, Li J, Liu X, Yeung KWK, Zheng Y, Cui Z, Yang X, Liang Y, Li Z, Zhu S, Yuan X, Feng X, Yang C, Wu S (2020) Enhanced photocatalytic activity and photothermal effects of Cu-doped metal-organic frameworks for rapid treatment of bacteria-infected wounds. Appl Catal B-Environ 261:118248
16. Li Y, Hu M, Huang X, Wang M, He L, Song Y, Jia Q, Zhou N, Zhang Z, Du M (2020) Multicomponent zirconium-based metal-organic frameworks for impedimetric aptasensing of living cancer cells. Sensor Actuat B-Chem 306:127608
17. Wang M, Hu M, Li Z, He L, Song Y, Jia Q, Zhang Z, Du M (2019) Construction of Tb-MOF-on-Fe-MOF conjugate as a novel platform for ultrasensitive detection of carbohydrate antigen 125 and living cancer cells. Biosens Bioelectron 142:111536
18. Cui J, Kan L, Li Z, Yang L, Wang M, He L, Lou Y, Xue Y, Zhang Z (2021) Porphyrin-based covalent organic framework as bioplatfrom for detection of vascular endothelial growth factor 165 through fluorescence resonance energy transfer. Talanta 228:122060
19. Wan S, Gándara F, Asano A, Furukawa H, Saeki A, Dey SK, Liao L, Ambrogio MW, Botros YY, Duan X, Seki S, Stoddart JF, Yaghi OM (2011) Covalent organic frameworks with high charge carrier mobility. Chem Mater 23:4094–4097
20. Allegrini F, Olivieri AC (2014) IUPAC-consistent approach to the limit of detection in partial least-squares calibration. Anal Chem 86:7858–7866
21. Yoo J, Lee S, Hirata S, Kim C, Lee CK, Shiraki T, Nakashima N, Shim JK (2015) In situ synthesis of covalent organic frameworks (COFs) on carbon nanotubes and graphenes by sonochemical reaction for CO_2 adsorbents. Chem Lett 44:560–562
22. Zhang A, Zhang H, Hu B, Wang M, Zhang S, Jia Q, He L, Zhang Z (2022) The intergrated nanostructure of bimetallic CoNi-based zeolitic imidazolate framework and carbon nanotubes as high-performance electrochemical supercapacitors. J Colloid Interf Sci 608:1257–1267
23. Peng Y, Huang Y, Zhu Y, Chen B, Wang L, Lai Z, Zhang Z, Zhao M, Tan C, Yang N, Shao F, Han Y, Zhang H (2017) Ultrathin two-dimensional covalent organic framework nanosheets: preparation and application in highly sensitive and selective DNA detection. J Am Chem Soc 139:8698–8704
24. Sarabaegi M, Roushani M, Hosseini H, Hoseini SJ, Bahrami M (2020) Facile synthesis of a covalent organic framework (COF) based on the reaction of melamine and trimesic acid incorporated electrospun nanofiber and its application as an electrochemical tyrosinamide aptasensor. New J Chem 44:14922–14927
25. Fragoso A, Laboria N, Latta D, O'Sullivan CK (2008) Electron permeable self-assembled monolayers of dithiolated aromatic scaffolds on gold for biosensor applications. Anal Chem 80:2556–2563
26. Fabian CP, Ridd MJ, Sheehan ME, Mandin P (2009) Modeling the charge-transfer resistance to determine the role of guar and activated polyacrylamide in copper electrodeposition. J Electrochem Soc 156:D400
27. Ru J, Hua Y, Wang D, Xu C, Li J, Li Y, Zhou Z, Gong K (2015) Mechanistic insight of in situ electrochemical reduction of solid PbO to lead in ChCl-EG deep eutectic solvent. Electrochim Acta 186:455–464
28. Zhang R-r, Li X-j, Sun A-l, Song S-q, Shi X-z (2022) A highly selective fluorescence nanosensor based on the dual-function molecularly imprinted layer coated quantum dots for the sensitive detection of diethylstilbestrol/cypermethrin in fish and seawater. Food Control 132:108438
29. Manzoor R, Wang L, Wang H, Lei Y, Sehrish A, Khan MS, Ali A, Wu D, Wei Q (2020) Ultrasensitive competitive electrochemiluminescence immunosensor based on luminol-AuNPs@Mo_2C and upconversion nanoparticles for detection of diethylstilbestrol. Microchem J 158:105283
30. Dong X, Zhao G, Liu L, Li X, Wei Q, Cao W (2018) Ultrasensitive competitive method-based electrochemiluminescence immunosensor for diethylstilbestrol detection based on $Ru(bpy)_3^{2+}$ as luminophor encapsulated in metal–organic frameworks UiO-67. Biosens Bioelectron 110:201–206
31. Liu S, Lin Q, Zhang X, He X, Xing X, Lian W, Li J, Cui M, Huang J (2012) Electrochemical immunosensor based on mesoporous nanocomposites and HRP-functionalized nanoparticles bioconjugates for sensitivity enhanced detection of diethylstilbestrol. Sensor Actuat B-Chem 166–167:562–568
32. Wu T, Yan T, Zhang X, Feng Y, Wei D, Sun M, Du B, Wei Q (2018) A competitive photoelectrochemical immunosensor for the detection of diethylstilbestrol based on an Au/UiO-66(NH_2)/CdS matrix and a direct Z-scheme Melem/CdTe heterojunction as labels. Biosens Bioelectron 117:575–582
33. Liu X, Hu Y, Sheng X, Peng Y, Bai J, Lv Q, Jia H, Jiang H, Gao Z (2017) Rapid high-throughput detection of diethylstilbestrol by using the arrayed langasite crystal microbalance combined with gold nanoparticles through competitive immunoassay. Sensor Actuat B-Chem 247:245–253
34. Shan Y, Zhang H-L, Zhu Y, Wang Y, Song H, Shi C (2020) Electrochemiluminescent CdTe nanocrystal/reduced graphene oxide composite films for the detection of diethylstilbestrol. ACS Appl Nano Mater 3:4670–4680
35. Chen P, Sun H, Wang X, Zhao Z, Pang Y (2012) Sensitive determination of diethylstilbestrol by high performance liquid chromatography with fluorescence detection with 4-(4,5-diphenyl-1H-imidazol-2-yl)benzoyl chloride as a labeling reagent. Anal Method 4:4049–4052